






Geophysical Research Letters[®]



RESEARCH LETTER

10.1029/2021GL095103

Landfast Ice and Coastal Wave Exposure in Northern Alaska

Lucia Hošeková¹ , Emily Eidam² , Gleb Pantelev³, Luc Rainville¹ , W. Erick Rogers³ , and Jim Thomson¹ 

¹Applied Physics Laboratory, University of Washington, Seattle, WA, USA, ²Department of Marine Sciences, University of North Carolina, Chapel Hill, NC, USA, ³Naval Research Laboratory, Stennis Space Center, MS, USA

Key Points:

- Year-long observations show a seasonal cycle of wave exposure at three sites along the Arctic coast of northern Alaska
- The persistence of landfast ice in the late spring/early summer dramatically reduces the wave energy reaching the coast
- Coastal protection by landfast ice is not represented in global climate models, but it can be parameterized

Supporting Information:

Supporting Information may be found in the online version of this article.

Correspondence to:

J. Thomson,
jthomson@apl.washington.edu

Citation:

Hošeková, L., Eidam, E., Pantelev, G., Rainville, L., Rogers, W. E., & Thomson, J. (2021). Landfast ice and coastal wave exposure in northern Alaska. *Geophysical Research Letters*, 48, e2021GL095103. <https://doi.org/10.1029/2021GL095103>

Received 20 JUL 2021

Accepted 5 NOV 2021

Author Contributions:

Conceptualization: Emily Eidam, Jim Thomson

Data curation: Lucia Hošeková, Gleb Pantelev, Luc Rainville, W. Erick Rogers

Formal analysis: Lucia Hošeková, W. Erick Rogers

Funding acquisition: Jim Thomson

Investigation: Lucia Hošeková

Methodology: Lucia Hošeková, Emily Eidam, W. Erick Rogers, Jim Thomson

Project Administration: Jim Thomson

© 2021 The Authors.

This is an open access article under the terms of the [Creative Commons Attribution-NonCommercial License](https://creativecommons.org/licenses/by/4.0/), which permits use, distribution and reproduction in any medium, provided the original work is properly cited and is not used for commercial purposes.

Abstract Observations of ocean surface waves at three sites along the northern coast of Alaska show a strong correlation with seasonal sea ice patterns. In the winter, ice cover is complete, and waves are absent. In the spring and early summer, sea ice retreats regionally, but landfast ice persists near the coast. The landfast ice completely attenuates waves formed farther offshore in the open water, causing up to a two-month delay in the onset of waves near shore. In autumn, landfast ice begins to reform, though the wave attenuation is only partial due to lower ice thickness compared to spring. The annual cycle in the observations is reproduced by the ERA5 reanalysis product, but the product does not resolve landfast ice. The resulting ERA5 bias in coastal wave exposure can be corrected by applying a higher-resolution ice mask, and this has a significant effect on the long-term trends inferred from ERA5.

Plain Language Summary Ocean waves facilitate coastal erosion in the Arctic (and worldwide). Wave energy reaching Arctic coasts is controlled by seasonal sea ice, which includes landfast ice attached to the coastlines or sea floor, and mobile pack ice further seaward. Wave energy in the Arctic is increasing due to the loss of pack ice, and these effects are generally well-represented in regional climate models. Landfast ice continues to form at the coast each year; when it lasts longer than pack ice, it provides protection against wave erosion. However, landfast ice is difficult to include in models which can lead them to overestimate the wave energy reaching the coasts. Using observations of waves from three coastal sites in Alaska, we demonstrate the importance of including landfast ice into regional models, and propose an effective method of combining public datasets to account for its effects on waves. These results can help the research community predict how much wave energy will be available for coastal erosion processes in the coming decades.

1. Introduction

Arctic coastlines experience rapid rates of erosion, up to tens of meters per year (Gibbs & Richmond, 2017; Jones et al., 2009). The mean retreat rate for coastlines throughout the Arctic is 0.5 m/yr (Lantuit et al., 2012), with the highest rates reported in the Laptev (Günther et al., 2013; Nielsen et al., 2020) and Beaufort Seas (Gibbs et al., 2015; Obu et al., 2017). The ice-rich soils are particularly sensitive to thermal niching by seawater at the coastal interface, a process which promotes failure of large blocks of ground along ice wedges (Aré, 1988a, 1988b; Hequette & Barnes, 1990; Günther et al., 2015). Incident wave energy and storm surges are considered dominant factors influencing the erosion rate, as these carry seawater into contact with ice-rich soils and mobilize nearshore sediments (Wobus et al., 2011). In recent decades, summertime pack ice extents in the Arctic have been declining, and the length of the open-water season has been increasing (Barnhart et al., 2016; Meier et al., 2013), a trend that is projected to continue. These changes have been linked to an increase in wave climate (Francis et al., 2011; Stopa et al., 2016; Thomson et al., 2016; Thomson & Rogers, 2014; Wang et al., 2015), and together these effects are expected to drive increasing rates of coastal erosion (Barnhart et al., 2014; Overeem et al., 2011).

Landfast ice buffers the coast against erosive wave energy, particularly during the spring, and, historically, during the summer (Forbes & Taylor, 1994). Landfast ice forms during the fall and generally remains attached to shore (and/or grounded to the seafloor in shallow water) during the winter, though changes in water level and other disturbances may cause it to shift (Mahoney et al., 2007). Recent observations suggest that landfast ice is becoming less stable and persists for briefer periods of time both at the beginning and end

Resources: Gleb Panteleev, Luc Rainville, W. Erick Rogers, Jim Thomson

Software: Lucia Hošeková, Jim Thomson

Supervision: Jim Thomson

Writing – original draft: Lucia Hošeková, W. Erick Rogers, Jim Thomson

Writing – review & editing: Lucia Hošeková, Emily Eidam, W. Erick Rogers, Jim Thomson

of the open-water season (Galley et al., 2012; Mahoney et al., 2014; Yu et al., 2014). Coastal wave exposure in the Arctic depends both on the distance to pack ice (i.e., the fetch), and on the presence of landfast ice dissipating the incident wave field. Global reanalysis products are used to evaluate the effects of waves on coastal erosion but do not explicitly account for landfast ice, leading to biases in projections of nearshore wave climates.

Here we present observations of wave conditions at three locations along the Alaskan coast throughout an annual cycle and use them to quantify the effects of landfast ice on coastal wave exposure. Section 2 includes a description of the sites, experimental setup, and datasets used in our analysis. In Section 3.1, we present observed significant wave heights in the context of local ice conditions. In Section 3.2, we compare the observed wave heights to the ERA5 dataset and propose a method to reduce its bias where and when landfast ice is present. In Section 4, we apply this approach to correct the estimated decadal trends in wave exposure in ECMWF Reanalysis v5 (ERA5) at one of the sites and discuss the processes driving seasonal break-up of landfast ice.

2. Methods

2.1. In-Situ Data Set

This study focuses on three nearshore sites representative of Arctic sandy barrier island systems (Figure 1a). The sites are in the vicinity of Icy Cape (Chukchi Sea), Jones Islands, and Flaxman Island (Beaufort Sea), and will be referred to as S1, S2, and S3 respectively. The mean long-term (>70 years) erosion rate of the exposed barrier coastlines in northern Alaska is estimated at 1.6 m/yr (± 0.73 m/yr) (Gibbs & Richmond, 2017).

Pairs of moorings were deployed at each site between November 2019 and September 2020, as part of the Coastal Ocean Dynamics in the Arctic (CODA) project. Each mooring pair consisted of a seafloor pressure and temperature logger (RBR Duo) located 3 nm (5.5 km) from the shore, and an acoustic Doppler current profiler (Nortek Signature500) on a seafloor tripod, which measured waves, currents, and temperature at a distance of 12 nm (22.2 km) from the shore. The moorings were positioned as a cross-shore array, and their locations are further referred to as “inshore” and “offshore”. The inshore sites were in 14–18 m water depth, and the offshore sites were in 25–30 m water depth. The mooring pairs provide a record of inshore and offshore conditions through a full annual cycle of coastal sea ice: freeze-up in the fall, full sea ice cover in winter, spring breakup, and open water in the summer months.

Wave energy spectra were estimated from the raw pressure and acoustic Doppler current profiler (ADCP) mooring data, collected at 1 Hz and processed every 30 min. The spectral processing uses 256-s windows and merges every three neighboring frequency bands, for an effective 42 degrees of freedom in the resulting spectral estimates. The frequency range used for analysis is $0.04 < f < 0.5$ Hz. The spectra from the RBR duo bottom pressure measurements at the inshore moorings are converted to sea-surface elevations using the frequency-dependent depth attenuation given by linear wave theory. The highest frequencies ($f > 0.3$ Hz) are too attenuated to measure with bottom pressure in 14–18 m water depth, and thus this portion of each spectrum is extrapolated to the highest frequency of 0.5 Hz using a canonical form f^{-4} . This is an upper bound on the energy at these frequencies because attenuation in sea ice will preferentially reduce this energy. Significant wave heights (H_s) are determined from the integral of the energy spectra, and the extrapolation is always less than a 10% adjustment to the reported significant wave height. At the offshore sites, this attenuation and extrapolation correction is unnecessary, because the Nortek Signature500 uses an acoustic altimeter to directly measure sea surface elevations at 1 Hz. For both instrument types, the minimum observable significant wave height is 0.05 m, based on an empirical determination of the noise floor in the spectra. Any 30-min record with a calculated H_s less than 0.05 m is considered to be a record without waves present.

Figures 1b–1e provide detail of the S1 location, the Icy Cape headland in the Chukchi Sea. The regional shoreline is largely erosional (-0.4 m/yr according to Gibbs et al., 2015), with strong variability in exposed shoreline change between the two sides of the headland (Gibbs et al., 2017; Snyder & Gibbs, 2019). The northeast-facing section is characterized by higher erosion rates (up to -4 m/yr), coinciding with its exposure to the prevailing wind and wave directions. Figures 1c and 1d show Synthetic-aperture radar (SAR)

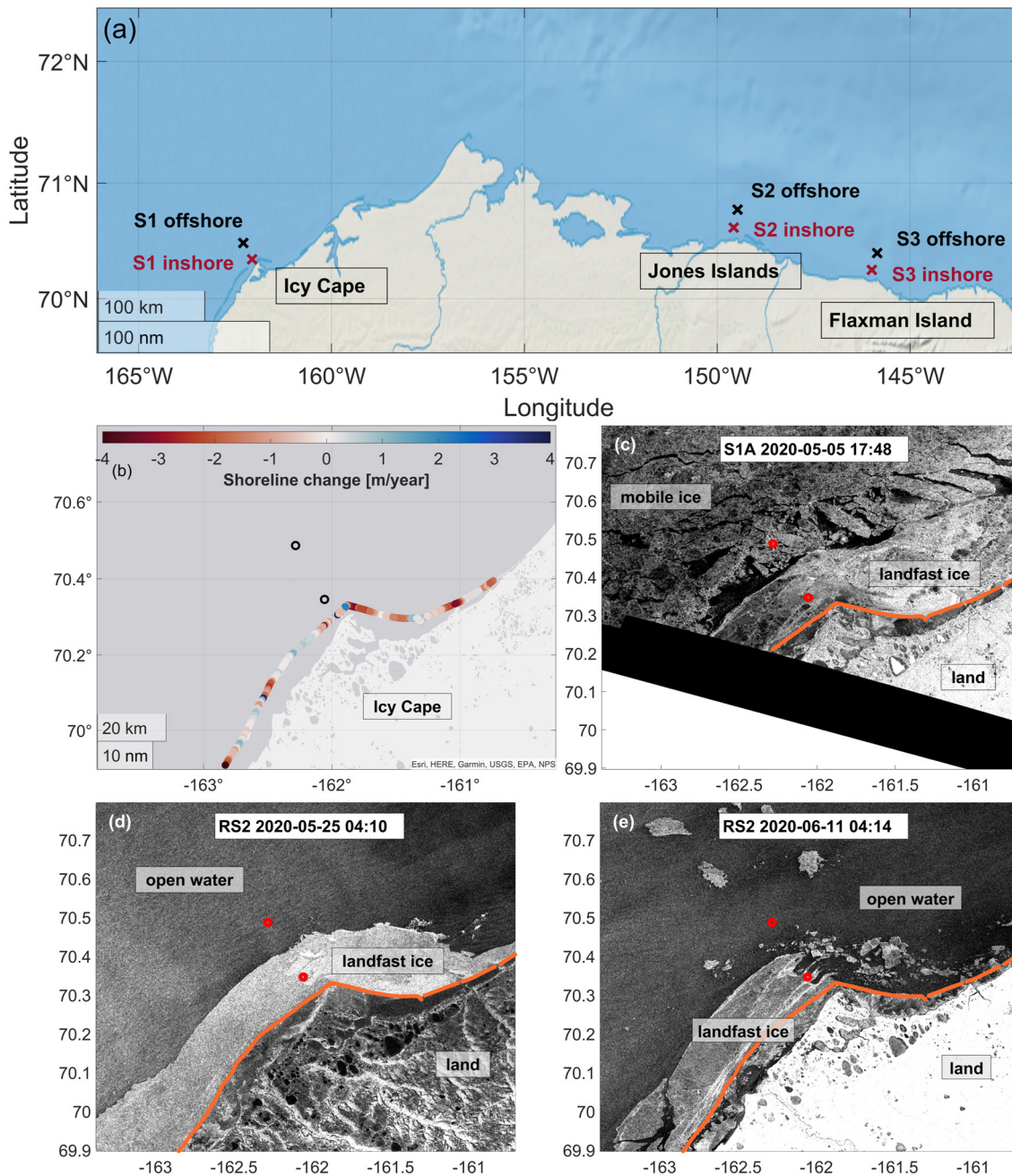


Figure 1. (a) Locations of the mooring sites S1, S2, and S3. (b) Detail of the S1 site, with colors representing rates of exposed shoreline change (Gibbs et al., 2017; Snyder & Gibbs, 2019). (c)–(e) Synthetic-aperture radar images acquired by Sentinel-1 and RADARSAT-2 capturing spring breakup of landfast ice in the Icy Cape area. Circles mark locations of S1 moorings. Orange line denotes the exposed shoreline.

images provided by Sentinel-1 and RADARSAT-2 detailing three stages of spring sea ice retreat at Icy Cape: 1. formation of the flaw lead 1(c) 2. exposed landfast ice 1(d) 3. break-up of landfast ice 1(e).

The 1 Hz acoustic altimeter data from the Nortek Signature500 sensors at the offshore moorings provide ice draft in addition to wave heights. This contextual data is not used directly in the present analysis, though it is consistent with the SAR images. In particular, the 30-min mean ice drafts increase throughout the winter to several meters in the months prior to the breakup. It is thus likely that the ice closer to shore is at least this thick in the late spring, where deformation and compaction along the coast are increasing the ice thickness beyond regional values (Fukamachi et al., 2017).

2.2. Ice and Wave Products

In Section 3.2, we compare the mooring wave observations to estimates from the atmospheric and wave reanalysis dataset ERA5 (Hersbach et al., 2020) at S1. ERA5 is produced by the European Center for Medium-Range Weather Forecasts (ECMWF) and provides hourly estimates of atmospheric data, including sea ice concentration, at 0.25° grid cell resolution (~30 km), and wave data at 0.5° resolution, and covers the period 1979-present. The ERA5 wave model WAM simulates wind-generated wave spectra with 24 directions and 30 frequencies when sea ice concentration is <30% and does not parametrize wave-ice interactions. While at 0.25° resolution ERA5 cannot distinguish individual positions of the mooring pairs located 16.6 km apart, it is chosen here as a convenient tool widely used to study multi-decadal evolution of wind, wave, and sea ice conditions in the Arctic (e.g., Casas-Prat & Wang, 2020; Kim et al., 2021).

In addition to ERA5, we utilize the sea ice concentration product obtained from GOFS 3.1 (Global Ocean Forecasting System, Metzger et al., 2014), the U.S. Navy's coupled global ocean-ice forecasting system. Its resolution is 0.08° longitude and 0.04° latitude (~5 km), allowing for a higher accuracy than ERA5 for indicating the presence of coastal sea ice. GOFS uses daily assimilation of passive microwave and other satellite ice products to reduce the accumulation of errors: this process is an update on the one described in Posey et al. (2015) and Hebert et al. (2015).

SAR satellite imagery provides a high resolution (~50 m) representation of the ice conditions every few days. Backscatter characteristics can be used to distinguish open water, sea ice floes, sea ice ridges, leads, and ice type with a high level of detail (e.g., Kwok et al., 1999).

Long-term trends in wave parameters (Section 4.1) are estimated by masking ERA5 with sea ice maps provided by the National Snow and Ice Data Center (NSIDC) as a weekly dataset. Sea ice categories are encoded according to the SIGRID-3 format and include landfast ice boundaries as a vector. The position of the landfast ice is extracted and re-mapped onto the GOFS 3.1 grid and interpolated to daily values.

2.3. Coastal Wave Exposure

Two metrics are used for evaluating the exposure of the coasts to the mechanical effects of surface waves. The first is a simple integration of observed and simulated significant wave heights, that is,

$$\mathcal{H} = \int H_s dt, \quad (1)$$

in units of meter-days, referred to as cumulative wave exposure. It provides an intuitive measure of wave activity and allows for a straightforward comparison between locations and datasets.

The second metric is the cumulative wave energy, which is calculated from the time integral of wave energy flux incident to the coast,

$$\mathcal{E} = \int E c_g dt, \quad (2)$$

in units of Joules per meter of shoreline. Here, incident means any wave energy directed toward the coast (as opposed to purely shore-normal energy). The time series of wave energy density E is determined as

$$E = \frac{\rho g H_s^2}{16}, \quad (3)$$

and the wave group velocity c_g is evaluated using the dispersion relation for intermediate water depth

$$c_g = \frac{L}{2T} + \frac{2\pi d}{T \sinh(4\pi d/L)}, \quad (4)$$

where ρ is the density of water, g is the gravitational acceleration, T is the energy period (first moment) of the reported energy spectrum, d is the water depth at the corresponding mooring location, and L is the wavelength calculated iteratively with inputs of energy period and depth.

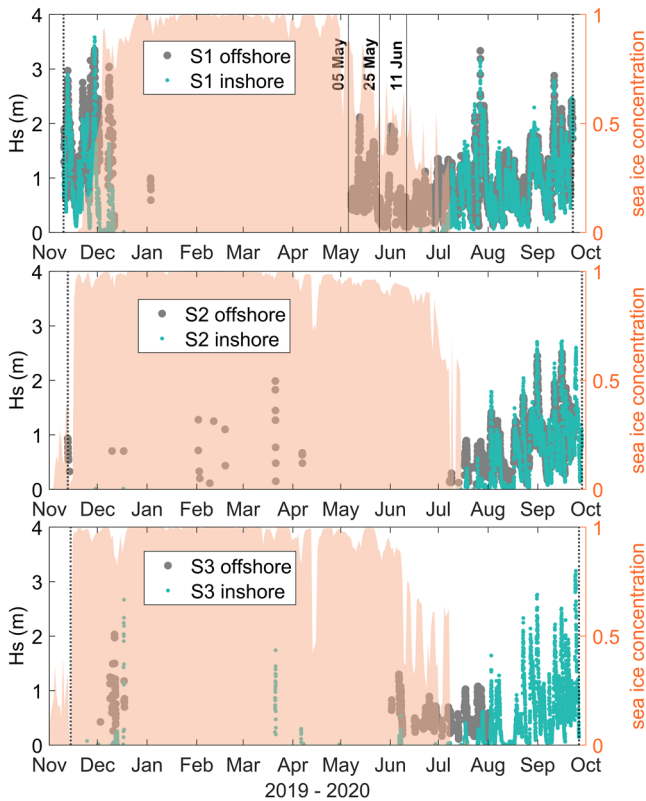


Figure 2. Significant wave heights observed by inshore and offshore moorings at S1, S2, and S3. Shaded orange area represents the mean daily sea ice concentration in a domain that includes both moorings as reported by GOFS. Black vertical lines mark dates of Synthetic-aperture radar imagery from Figure 1. Dotted black lines mark dates of mooring deployments and recoveries. Ticks on the horizontal axis correspond to the first day of the month. The S3 offshore dataset concludes prematurely in August 2020 due to equipment failure.

3. Results

3.1. Wave Height Observations

Significant wave heights at the mooring locations (Figure 1) are shown in Figure 2. In the summer months with low sea ice concentrations, significant wave heights are up to 3 m at all sites, consistent with the wave climatology for the region (Stopa et al., 2016; Thomson et al., 2016). In the winter months with high sea ice concentrations, waves are generally not observed, although there are a few isolated wave events in the winter. In the spring with moderate sea concentrations, waves are observed offshore, but not inshore.

At S1, both moorings were deployed mid-November 2019 in open water. A series of energetic wave events in November and December coincided with the onset of nearshore pancake sea ice covering the S1 inshore mooring (Hošeková et al., 2020), resulting in partial wave attenuation. The Icy Cape region was fully ice-covered from mid-December until the beginning of May and only sporadic wave activity was detected during this period. In the following two months, the offshore mooring recorded continuous-wave activity with significant wave heights of up to 2 m, in contrast to no detectable waves at the inshore mooring location. Satellite imagery obtained using RADARSAT-2 and Sentinel-1 shows a continuous presence of landfast ice during this period (Figures 1d and 1e), implying complete attenuation of wave energy between the two mooring sites. At the beginning of July, the landfast ice covering the inshore mooring rapidly breaks up and the subsequent wave measurements at the two locations are in agreement for the remainder of the open water season.

At S2, the moorings were deployed during autumn 2019 ice formation and remained mostly covered by ice until the beginning of July 2020. As at S1, the inshore location was collocated with landfast ice, while the offshore site was covered by mobile ice. On occasion, a flaw lead formed between landfast ice and pack ice and led to sporadic waves detected offshore (only). At the beginning of July, the pack ice retreated and the landfast ice broke off in close succession, resulting in a rapid transition to open water over the period of a week. Waves up to 1 m were detected during this time and were partially attenuated at the inshore location.

At S3, the flaw lead between landfast ice and pack ice formed a month earlier than at S2 (140 km to the west), allowing for waves to reach the offshore mooring location in early July. As at the other sites, the presence of landfast ice over the inshore mooring led to complete attenuation of the incident wave field. SAR imagery reveals deterioration of the landfast ice at the S3 location through a series of break-up events (see Supporting Information S1), leaving both mooring locations ice-free by the beginning of July.

The above inference of “complete attenuation” refers to the situation where the wave energy level has become so small that it can no longer be measured using our instrumentation ($H_s < 0.05$ m) and effectively there are no waves at the inshore mooring. In situ observations of attenuation in landfast ice is not common, and this result of complete attenuation is unusual relative to pack ice in deep water (Ardhuin et al., 2017; Cheng et al., 2020). Sutherland and Rabault (2016) did make observations in landfast ice and reported a 12% energy reduction at $f = 0.15$ Hz over a distance of 60 m. Although the ice in our study is much thicker, we can use the Sutherland and Rabault (2016) attenuation rate to assess the theoretical attenuation between the offshore and onshore moorings. The resulting prediction is for $H_s = 2$ m to reduce to the detection threshold of $H_s = 0.05$ m over a distance of 3.4 km. Given the SAR imagery (Figure 1) showing roughly 8 km of landfast ice at Icy Cape, the inference of “complete attenuation” is indeed reasonable.

Observations from all three sites include a few winter wave events. These are beyond the scope of this paper, though such events may be important to sea ice breakup and sea ice dynamics in general (Ardhuin et al., 2020; Johnson et al., 2021; Stopa et al., 2018). Examination of the wave spectra (not shown) from these brief events suggests that a local wind-sea develops within an open lead near the coast. Such leads are not resolved in the sea ice concentration time series, however, they are visible in some of the weekly SAR images. The late winter events may be specific to this particular year, as there were several major cyclones in the region coincident with the collapse of the Beaufort High (Ballinger et al., 2021).

The CODA dataset demonstrates that coastal waves during the spring transition are limited by both the distance of the offshore ice edge controlling the available wind fetch, and by the presence of landfast ice which prevents the waves from reaching the coast. The contrast between these two factors is particularly evident in the Beaufort Sea locations (S2 and S3) where the onset of offshore waves matches the increasing gap between landfast ice and the drifting pack ice, while the onset of inshore waves is determined by the local break-up of landfast ice and occurs almost simultaneously at both sites.

3.2. Comparison With ERA5 at S1

In this section, we compare the CODA dataset at the Chukchi Sea location S1 with ERA5 reanalysis products, and we consider a modification using the GOFS ice products to make the ERA5 results more consistent with the in situ inshore wave observations. The S1 site was chosen for two reasons: CODA measurements here provide a clear signal contrasting the high wave activity offshore to complete wave attenuation nearshore, correlating with the presence of landfast ice; and the rapid decrease in duration of landfast ice reported along the Chukchi coast (4 weeks/decade, Yu et al., 2014) highlights its relevance in coastal erosion processes in the region. The results from S2 and S3 are qualitatively similar, though less striking in magnitude. Such site-specific behaviors likely are related to the size and persistence of a fetch for wave generation between the landfast ice and the offshore pack ice.

ERA5 data presented in this section are evaluated hourly at the nearest grid point to the S1 site. The observations are linearly interpolated to the same times. The GOFS dataset was downloaded for daily increments at the time the model assimilates new data (12:00 UTC) and interpolated it to hourly intervals.

Figure 3a presents the significant wave heights recorded by the two S1 moorings compared to ERA5 output over spring and summer 2020. Overall, the ERA5 dataset is in good agreement with the wave heights measured by the offshore mooring throughout the entire period, with a brief exception in the spring when there is some ice in the model grid cell but none right at the mooring location. More importantly, ERA5 does not reproduce the difference between the onset of wave activity at the inshore and offshore location, causing a significant overestimate of inshore waves by ERA5 that persists for two months. This is because both mooring sites are effectively located within a single ERA5 grid cell, and no significant sea ice presence is reported by ERA5 during these months.

The black line in Figure 3a demonstrates that the absence of landfast ice in ERA5 can be rectified by applying a higher resolution sea ice product (i.e., GOFS, see Section 2.2) to mask the waves in the nearshore. The mask here is applied when the mean sea ice concentration exceeds 0% within the GOFS grid cells that bound the inshore mooring location. This approach is based on two assumptions: (a) waves incident from offshore are completely attenuated and (b) the nearshore ice cover reported by GOFS during spring transition can be considered to be fast ice, even though the GOFS dataset does not explicitly distinguish between ice types. The first assumption is supported by observations. The second assumption is supported by SAR imagery of the CODA sites for the duration of the experiment (see Supporting Information S1), though it may not apply as well to other sites without supporting SAR imagery.

Figure 3b shows the cumulative wave exposure (Equation 1) for May through mid-August 2020, as reported by the S1 mooring pair, the ERA5 dataset, and ERA5 data corrected using the GOFS sea ice concentration as outlined above. The wave exposure metric illustrates the role of landfast ice presence in preventing waves from reaching the coastline: by mid-August, the cumulative wave exposure at the inshore location amounted to 46% of that measured offshore. The value reported by ERA5 closely tracks the offshore dataset, while ERA5 in combination with the GOFS mask provides a wave exposure estimate resembling the inshore measurements (47% of the offshore value by mid-August). Correcting ERA5 using a high resolution sea ice

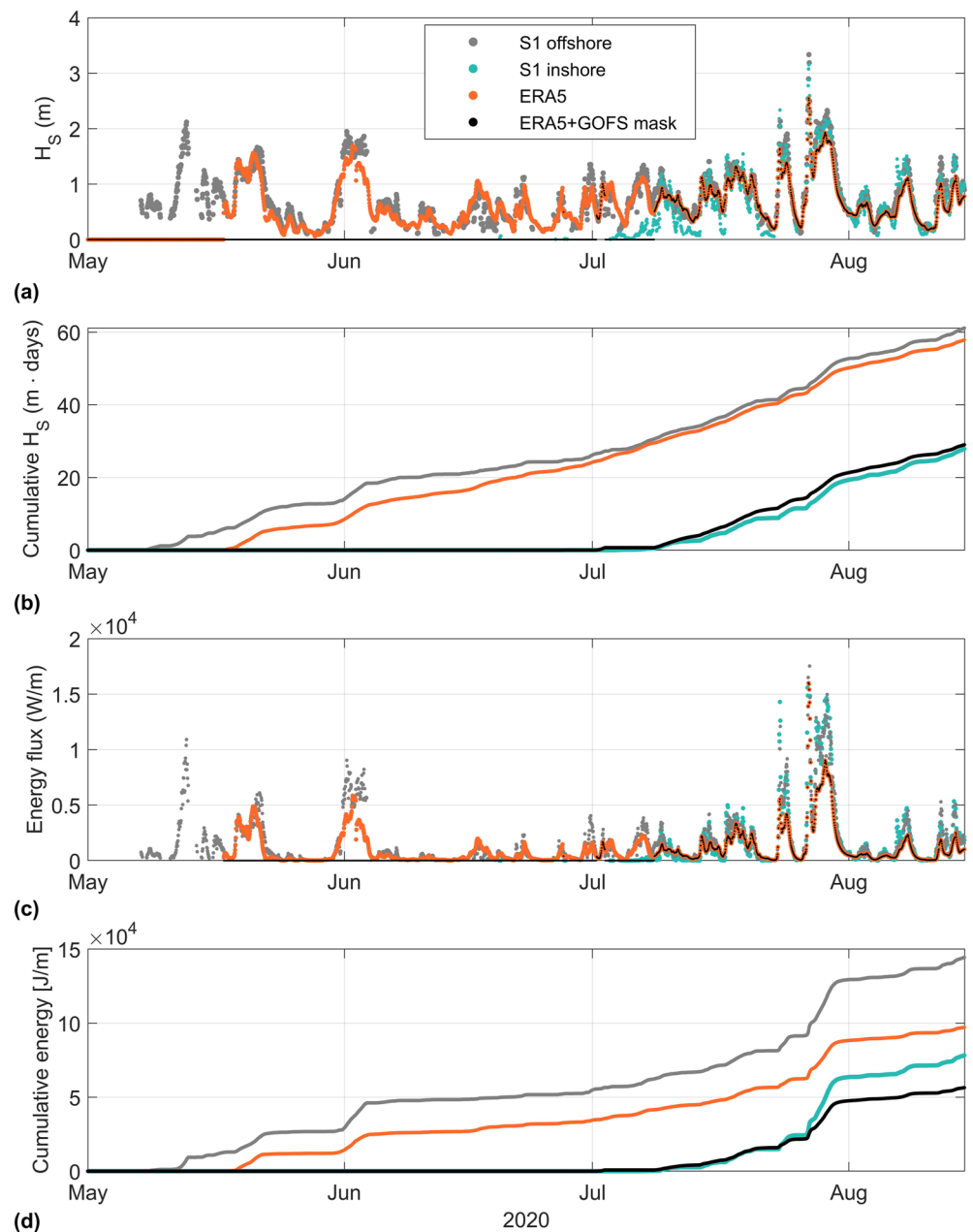


Figure 3. (a) Comparison of observed significant wave heights at S1 and ERA5 reanalysis with and without GOFs sea ice presence mask. All data is interpolated to 1 hr intervals. (b) Daily cumulative sum of wave heights between May 1 - August 15, 2020. (c) Same as (a) for observed wave energy flux. (d) Same as (c), accumulated daily between May 1 and August 15, 2020.

product (or ideally, a landfast-ice product) provides more realistic coastal wave exposure than using ERA5 data alone. This bias in ERA5 is somewhat expected, given the assimilation of satellite microwave products that are biased near the coasts (Meier & Stewart, 2019) and the coarse resolution of the ERA5 products.

Figure 3 further shows the energy flux (c) and cumulative wave energy (d) incident to the Icy Cape headland as reported by instruments at S1 and ERA5 dataset between May - mid-August 2020. The geometry of the headland is taken into account and non-incident wave spectra are discarded (i.e., only the range of $220^\circ < \theta < 100^\circ$ is included). Estimates of wave direction are only available from the offshore mooring, and are used at both mooring locations. Just as shown for the wave exposure metric in Figure 3b, the presence of

landfast ice significantly reduces the cumulative wave energy arriving at the inshore location, by approximately 54% over the spring and summer season.

ERA5 tends to underpredict the offshore energy flux associated with individual wave events (Figure 3c), despite its good agreement with offshore H_s measurements (Figure 3a). Consequently, only 67% of the total observed offshore energy is reported by ERA5 at the end of the studied time window (Figure 3d). While this is closer to the values observed inshore, it is attributed to additional model biases in wave direction and the mean period, rather than an effect of wave attenuation by landfast ice. Accounting for landfast ice presence by applying a GOFS mask, the ERA5 cumulative energy prediction is further reduced to only 39% of the offshore value, considerably lower than the observed 54% inshore.

4. Discussion

Here we discuss the implications and limitations of these results for understanding long-term trends and coastal processes. ERA5 is quickly becoming a widely used resource, and there is a related need to ensure that unresolved processes do not cause large biases in results derived from it. The approach is motivated by the strong agreement of ERA5 waves with in situ observations for an entire year at multiple sites, *except* when landfast ice persists longer than offshore pack ice (a period which presently lasts approximately 2 months).

4.1. Long-Term Trends at S1

The wave observations in Figure 2 suggest that the presence of landfast ice can cause a substantial delay in the spring onset of wave activity along the Alaskan coasts, relative to the seasonal emergence of waves offshore. While the offshore wave energy and number of open water days are increasing in recent decades (Thomson et al., 2016), it is unclear to what extent this trend is moderated by landfast ice near the coast. Here we explore 41-year long trends in wave presence (as a proxy for open water days), wave exposure, and cumulative energy at S1 estimated using ERA5, and apply a correction to account for landfast ice presence based on the masking method outlined in Section 3.2 (Figure 4).

ERA5 datasets for the significant wave height, mean wave period based on the first moment and mean wave direction are downloaded at 6-hourly intervals and averaged to obtain daily means for the time period 1979–2020. Because the GOFS sea ice dataset used in Section 3.2 only extends from December 2018 to the present and does not explicitly classify landfast ice, we use weekly rasterized landfast ice products from NSIDC (see Section 2.2) instead, covering years 2009–2020.

The long-term ERA5 datasets show evidence of increasing trends in the number of open water days (5.8 ± 1.3 days/year), wave exposure (5.1 ± 1.7 days·m/year), and cumulative wave energy ($1.6 \times 10^4 \pm 1.1 \times 10^4$ J/(m·year)). Despite high inter-annual variability, the trends are qualitatively consistent with other studies showing a comparative increase in open water days and wave heights (Thomson et al., 2016).

Introduction of the landfast ice mask to ERA5 data at S1 leads to a statistically significant reduction in trend estimates over 2009–2020, despite uncertainties related to inter-annual variability and limited temporal resolution of the landfast ice dataset. The correction is significant to the annual trends, even though the landfast ice mask only corrects a few months per year. The corrected nearshore trends are 1.6 ± 1.2 days/year for number of open water days, 1.6 ± 1.3 days·m/year for wave exposure, and $3.5 \times 10^3 \pm 6.5 \times 10^3$ J/(m·year) for cumulative wave energy. This is of particular relevance to studies that rely on reanalysis datasets and model projections to evaluate long-term erosive effects of waves.

4.2. Spring Break-Up of Landfast Ice

Expanding these methods beyond a simple ice-mask will require more detailed treatment of the landfast ice processes and coupling with other coastal processes. Coastal protection by landfast ice is intrinsically tied to the evolution of the ice itself. When landfast ice is present, the seawater temperatures are maintained at or near the freezing point, and processes such as thermal niching of permafrost bluffs are inhibited. The

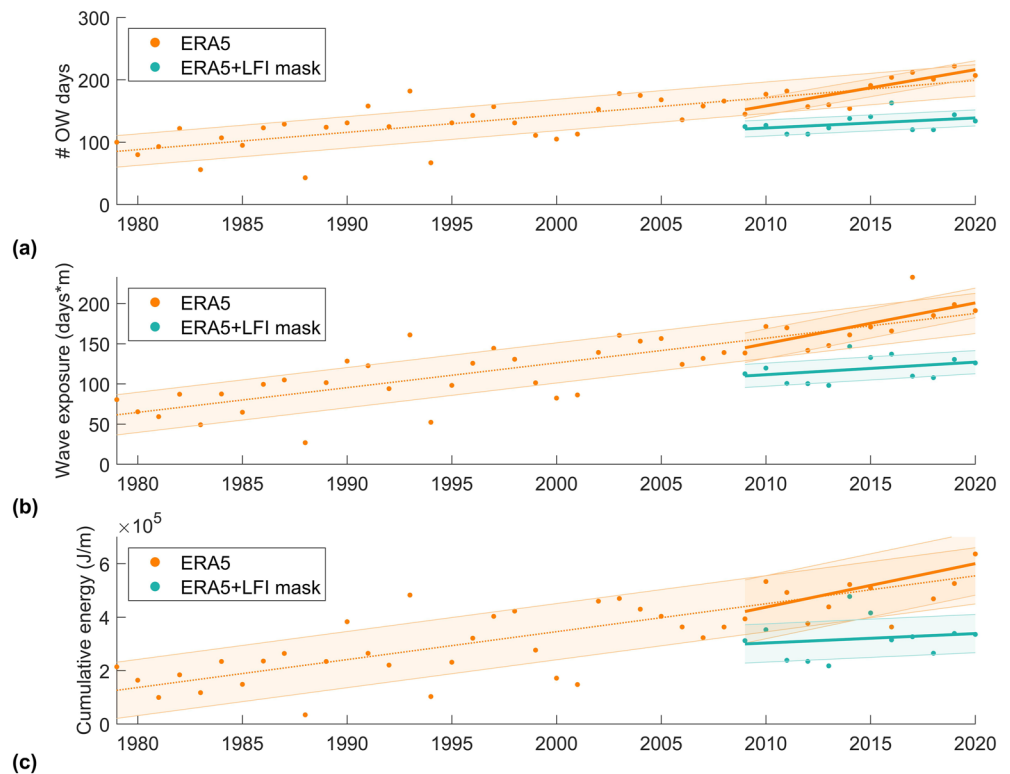


Figure 4. (a) Number of open water days at S1 reported by ERA5 with and without correcting for landfast ice (green and orange, respectively). (b) Same as (a) for coastal wave exposure at S1. (c) Same as (a) for cumulative energy incident to Icy Cape headland. Trend lines are evaluated using linear regression for 1979–2020 (dotted) and 2009–2020 (solid). Shaded areas correspond to standard error of the regression.

seasonal breakout of landfast ice can be driven by either mechanical (waves, winds, currents) or thermal (solar radiation, advected/upwelled warm water) forcing. Solar radiation is thought to be the most important driver (Petrich et al., 2012), however multiple feedbacks are possible, including the grounding of the landfast ice in shallow water that may enhance persistence at specific sites. The CODA dataset includes observations of rapid increases in water temperature coincident with the retreat of the landfast ice (see Supporting Information S1), though it is not clear if this is a cause or a consequence. The clear signal reported and applied here is simply that landfast ice causes persistent coastal protection from wave action that is not resolved by global climate models. Whether this modulation of coastal wave exposure is an essential factor in the retreat of permafrost shorelines is still to be determined.

5. Conclusions

Observations of ocean surface waves at multiple sites along the Arctic coast of Alaska demonstrate that:

1. The seasonal wave climate is controlled by both the distance from pack ice (i.e., regional fetch) and the attenuation within nearshore (landfast) ice.
2. Wave onset at the coast is delayed by landfast ice. During the spring melt season, we observed complete attenuation of the incident wave field by landfast ice, delaying wave activity at the shoreline by up to 60 days.
3. While the ERA5 reanalysis shows good agreement with observed offshore wave heights, it fails to reproduce the delayed wave onset at the coast caused by unresolved landfast ice. This results in ERA5 overestimating the cumulative spring coastal wave exposure by up to 47% compared to observations.
4. Applying a landfast ice mask derived from a high resolution sea ice product (e.g., GOFs, NIC) to ERA5 significantly reduces the bias in reported wave exposure and number of open water days.

5. The lack of landfast ice information causes ERA5 to overestimate the inter-annual trend in the number of open water days by (i.e., days with no ice at the coast) up to 72% at the Chukchi Sea coast.

These results can be applied to improve understanding of coastal change in the emerging Arctic, though the details of key coastal processes remain obscure.

Data Availability Statement

Data are available from <http://hdl.handle.net/1773/47139>. ERA5 results are available at <https://cds.climate.copernicus.eu/>. Sea ice maps are available at <http://wdc.aari.ru/datasets/d0032/arctic/>.

Acknowledgments

Alex de Klerk and the crew of *R/V Sikuliaq* helped with data collection. Nirni Kumar helped initiate the project and focus our efforts. John and Becca Guillote documented our work on www.iceinmotion.com. L. Hosekova and J. Thomson were funded by US National Science Foundation (OPP, 1818485). G. Pantelev and E. Rogwers were funded by the Office of Naval Research, Program Elements 62435 and 0601153N. L. Rainville was funded by the Office of Naval Research grant N000141612377. Satellite ice images and analysis were provided via special support from the U.S. National Ice Center. RADARSAT-2 Data and Products are under copyright of MDA Geospatial Services Inc. 2019–2020—All Rights Reserved, obtained via the U.S. National Ice Center. RADARSAT is an official mark of the Canadian Space Agency.

References

- Ardhuin, F., Otero, M., Merrifield, S., Grouazel, A., & Terrill, E. (2020). Ice break-up controls dissipation of wind-waves across southern ocean sea ice. *Geophysical Research Letters*, *47*, e2020GL087699. <https://doi.org/10.1029/2020GL087699>
- Ardhuin, F., Stopa, J., Chapron, B., Collard, F., Smith, M., Thomson, J., et al. (2017). Measuring ocean waves in sea ice using {SAR} imagery: A quasi-deterministic approach evaluated with sentinel-1 and in situ data. *Remote Sensing of Environment*, *189*, 211–222. <https://doi.org/10.1016/j.rse.2016.11.024>
- Aré, F. E. (1988a). Thermal abrasion of sea coasts (Part I). *Polar Geography and Geology*, *12*(1). <https://doi.org/10.1080/10889378809377343>
- Aré, F. E. (1988b). Thermal abrasion of sea coasts (Part II). *Polar Geography and Geology*, *12*(2), 87–87. <https://doi.org/10.1080/10889378809377352>
- Ballinger, T. J., Walsh, J. E., Bhatt, U. S., Bieniek, P. A., Tschudi, M. A., Bretschneider, B., & Shapiro, L. H. (2021). Unusual west arctic storm activity during winter 2020: Another collapse of the Beaufort high? *Geophysical Research Letters*, *48*(13), e2021GL092518. <https://doi.org/10.1029/2021gl092518>
- Barnhart, K. R., Miller, C. R., Overeem, I., & Kay, J. E. (2016). Mapping the future expansion of Arctic open water. *Nature Climate Change*, *36*, 280–285. <https://doi.org/10.1038/nclimate2848>
- Barnhart, K. R., Overeem, I., & Anderson, R. S. (2014). The effect of changing sea ice on the physical vulnerability of Arctic coasts. *The Cryosphere*, *8*(5), 1777–1799. <https://doi.org/10.5194/tc-8-1777-2014>
- Casas-Prat, M., & Wang, X. L. (2020). Projections of extreme ocean waves in the Arctic and potential implications for coastal inundation and erosion. *Journal of Geophysical Research: Oceans*, *125*(8), e2019JC015745. <https://doi.org/10.1029/2019JC015745>
- Cheng, S., Stopa, J., Ardhuin, F., & Shen, H. H. (2020). Spectral attenuation of ocean waves in pack ice and its application in calibrating viscoelastic wave-in-ice models. *The Cryosphere*, *14*(6), 2053–2069. <https://doi.org/10.5194/tc-14-2053-2020>
- Forbes, D., & Taylor, R. (1994). Ice in the shore zone and the geomorphology of cold coasts. *Progress in Physical Geography: Earth and Environment*, *18*(1), 59–89. <https://doi.org/10.1177/03091333940180010410.1177/030913339401800104>
- Francis, O. P., Pantelev, G. G., & Atkinson, D. E. (2011). Ocean wave conditions in the Chukchi Sea from satellite and in situ observations. *Geophysical Research Letters*, *38*, L24610. <https://doi.org/10.1029/2011GL049839>
- Fukamachi, Y., Simizu, D., Ohshima, K. I., Eicken, H., Mahoney, A. R., Iwamoto, K., et al. (2017). Sea-ice thickness in the coastal northeastern chukchi sea from moored ice-profiling sonar. *Journal of Glaciology*, *63*(241), 888–898. <https://doi.org/10.1017/jog.2017.56>
- Galley, R. J., Else, B. G., Howell, S. E., Lukovich, J. V., & Barber, D. G. (2012). Landfast sea ice conditions in the Canadian Arctic: 1983–2009. *Arctic*, *66*(5), 133–144. <https://doi.org/10.14430/arctic4195>
- Gibbs, A. E., Ohman, K. A., Coppersmith, R., & Richmond, B. M. (2017). *A GIS compilation of updated vector shorelines and associated shoreline change data for the north coast of Alaska, U.S. Canadian border to Icy Cape*. U.S. Geological Survey data release. <https://doi.org/10.5066/F72Z13N1>
- Gibbs, A. E., Ohman, K. A., & Richmond, B. M. (2015). *National assessment of shoreline change—a GIS compilation of vector shorelines and associated shoreline change data for the north coast of Alaska, U.S.-Canadian border to Icy Cape (Open-File Report No. 2015-1030)*. U.S. Geological Survey. <https://doi.org/10.3133/ofr20151030>
- Gibbs, A. E., & Richmond, B. M. (2017). *National assessment of shoreline change—Summary statistics for updated vector shorelines and associated shoreline change data for the north coast of Alaska, U.S. Canadian border to icy Cape: U.S. geological survey open-file report 2017-1107 (Open-File report No. 2017-1107)*. U.S. Geological Survey. <https://doi.org/10.3133/ofr20171107>
- Günther, F., Overduin, P. P., Sandakov, A. V., Grosse, G., & Grigoriev, M. N. (2013). Short- and long-term thermo-erosion of ice-rich permafrost coasts in the Laptev Sea region. *Biogeosciences*, *10*(6), 4297–4318. <https://doi.org/10.5194/bg-10-4297-2013>
- Günther, F., Overduin, P. P., Yakshina, I. A., Opel, T., Baranskaya, A. V., & Grigoriev, M. N. (2015). Observing Muostakh disappear: Permafrost thaw subsidence and erosion of a ground-ice-rich island in response to Arctic summer warming and sea ice reduction. *The Cryosphere*, *9*(1), 151–178. <https://doi.org/10.5194/tc-9-151-2015>
- Hebert, D. A., Allard, R. A., Metzger, E. J., Posey, P. G., Preller, R. H., Wallcraft, A. J., et al. (2015). Short-term sea ice forecasting: An assessment of ice concentration and ice drift forecasts using the US Navy's Arctic Cap Nowcast/Forecast System. *Journal of Geophysical Research: Oceans*, *120*(12), 8327–8345. <https://doi.org/10.1002/2015JC011283>
- Hequette, A., & Barnes, P. W. (1990). Coastal retreat and shoreface profile variations in the Canadian Beaufort sea. *Marine Geology*, *91*(1), 113–132. [https://doi.org/10.1016/0025-3227\(90\)90136-8](https://doi.org/10.1016/0025-3227(90)90136-8)
- Hersbach, H., Bell, B., Berrisford, P., Hirahara, S., Horányi, A., Muñoz-Sabater, J., et al. (2020). The ERA5 global reanalysis. *Quarterly Journal of the Royal Meteorological Society*, *146*(730), 1999–2049. <https://doi.org/10.1002/qj.3803>
- Hošeková, L., Malila, M. P., Rogers, W. E., Roach, L. A., Eidam, E., Rainville, L., et al. (2020). Attenuation of ocean surface waves in pancake and frazil sea ice along the coast of the Chukchi Sea. *Journal of Geophysical Research: Oceans*, *125*(12), e2020JC016746. <https://doi.org/10.1029/2020JC016746>
- Johnson, M. A., Marchenko, A. V., Dammann, D. O., & Mahoney, A. R. (2021). Observing wind-forced flexural-gravity waves in the Beaufort Sea and their relationship to sea ice mechanics. *Journal of Marine Science and Engineering*, *9*(5). <https://doi.org/10.3390/jmse9050471>
- Jones, B. M., Arp, C. D., Jorgenson, M. T., Hinkel, K. M., Schmutz, J. A., & Flint, P. L. (2009). Increase in the rate and uniformity of coastline erosion in Arctic Alaska. *Geophysical Research Letters*, *36*(3), L03503. <https://doi.org/10.1029/2008GL036205>

- Kim, J., Murphy, E., Nistor, I., Ferguson, S., & Provan, M. (2021). Numerical analysis of storm surges on Canada's western arctic coastline. *Journal of Marine Science and Engineering*, 9(3). <https://doi.org/10.3390/jmse9030326>
- Kwok, R., Cunningham, G. F., LaBelle-Hamer, N., Holt, B., & Rothrock, D. (1999). Ice thickness derived from high-resolution radar imagery. *Eos, Transactions American Geophysical Union*, 80(42), 495–497. <https://doi.org/10.1029/eo080i042p00495-01>
- Lantuit, H., Overduin, P. P., Couture, N., Wetterich, S., Aré, F., Atkinson, D., et al. (2012). The Arctic coastal dynamics database: A new classification scheme and statistics on Arctic permafrost coastlines. *Estuaries and Coasts*, 35(2), 383–400. <https://doi.org/10.1007/s12237-010-9362-6>
- Mahoney, A., Eicken, H., & Shapiro, L. (2007). How fast is landfast sea ice? A study of the attachment and detachment of nearshore ice at Barrow, Alaska. *Cold Regions Science and Technology*, 47(3), 233–255. <https://doi.org/10.1016/j.coldregions.2006.09.005>
- Mahoney, A. R., Eicken, H., Gaylord, A. G., & Gens, R. (2014). Landfast sea ice extent in the Chukchi and Beaufort Seas: The annual cycle and decadal variability. *Cold Regions Science and Technology*, 103, 41–56. <https://doi.org/10.1016/j.coldregions.2014.03.003>
- Meier, W. N., Gallaher, D., & Campbell, G. G. (2013). New estimates of Arctic and Antarctic sea ice extent during September 1964 from recovered Nimbus I satellite imagery. *The Cryosphere*, 7, 699–705. <https://doi.org/10.5194/tc-7-699-2013>
- Meier, W. N., & Stewart, J. S. (2019). Assessing uncertainties in sea ice extent climate indicators. *Environmental Research Letters*, 14(3), 035005. <https://doi.org/10.1088/1748-9326/aaf52c10.1088/1748-9326/aaf52c>
- Metzger, E. J., Smedstad, O. M., Thoppil, P. G., Hurlburt, H. E., Cummings, J. A., Wallcraft, A. J., et al. (2014). US Navy Operational Global Ocean and Arctic Ice Prediction Systems. *Oceanography*, 27, 32–43. <https://doi.org/10.5670/oceanog.2014.66>
- Nielsen, D. M., Dobrynin, M., Baehr, J., Razumov, S., & Grigoriev, M. (2020). Coastal erosion variability at the southern Laptev Sea linked to winter sea ice and the Arctic oscillation. *Geophysical Research Letters*, 47(5), e2019GL086876. <https://doi.org/10.1029/2019GL086876>
- Obu, J., Lantuit, H., Grosse, G., Günther, F., Sachs, T., Helm, V., & Fritz, M. (2017). Coastal erosion and mass wasting along the Canadian Beaufort Sea based on annual airborne LiDAR elevation data. *Geomorphology*, 293, 331–346. <https://doi.org/10.1016/j.geomorph.2016.02.014>
- Overeem, I., Anderson, R. S., Wobus, C. W., Clow, G. D., Urban, F. E., & Matell, N. (2011). Sea ice loss enhances wave action at the Arctic coast. *Geophysical Research Letters*, 38(17). <https://doi.org/10.1029/2011GL048681>
- Petrich, C., Eicken, H., Zhang, J., Krieger, J., Fukamachi, Y., & Ohshima, K. I. (2012). Coastal landfast sea ice decay and breakup in northern Alaska: Key processes and seasonal prediction. *Journal of Geophysical Research: Oceans*, 117(C2). <https://doi.org/10.1029/2011jc007339>
- Posey, P. G., Metzger, E. J., Wallcraft, A. J., Hebert, D. A., Allard, R. A., Smedstad, O. M., et al. (2015). Improving Arctic sea ice edge forecasts by assimilating high horizontal resolution sea ice concentration data into the US Navy's ice forecast systems. *The Cryosphere*, 9(4), 1735–1745. <https://doi.org/10.5194/tc-9-1735-2015>
- Snyder, A. G., & Gibbs, A. E. (2019). *National assessment of shoreline change: A GIS compilation of updated vector shorelines and associated shoreline change data for the north coast of Alaska, icy Cape to Cape Prince of Wales*. U.S. Geological Survey. <https://doi.org/10.5066/P9H1S1PV>
- Stopa, J. E., Arduhin, F., & Girard-Adrhun, F. (2016). Wave-climate in the Arctic 1992–2014: Seasonality, trends, and wave-ice influence. *The Cryosphere*, 10(4), 1605–1629. <https://doi.org/10.5194/tc-10-1605-2016>
- Stopa, J. E., Sutherland, P., & Arduhin, F. (2018). Strong and highly variable push of ocean waves on southern ocean sea ice. *Proceedings of the National Academy of Sciences*, 115(23), 5861–5865. <https://doi.org/10.1073/pnas.1802011115>
- Sutherland, G., & Rabault, J. (2016). Observations of wave dispersion and attenuation in landfast ice. *Journal of Geophysical Research: Oceans*, 121, 1984–1997. <https://doi.org/10.1002/2015JC011446>
- Thomson, J., Fan, Y., Stammerjohn, S., Stopa, J., Rogers, W. E., Girard-Adrhun, F., et al. (2016). Emerging trends in the sea state of the Beaufort and Chukchi seas. *Ocean Modelling*, 105, 1–12. <https://doi.org/10.1016/j.ocemod.2016.02.009>
- Thomson, J., & Rogers, W. E. (2014). Swell and sea in the emerging Arctic Ocean. *Geophysical Research Letters*, 41, 3136–3140. <https://doi.org/10.1002/2014GL059983>
- Wang, X. L., Feng, Y., Swail, V. R., & Cox, A. (2015). Historical changes in the Beaufort-Chukchi-Bering seas surface winds and waves, 1971–2013. *Journal of Climate*, 28, 7457–7469. <https://doi.org/10.1175/JCLI-D-15-0190.1>
- Wobus, C., Anderson, R., Overeem, I., Matell, N., Clow, G., & Urban, F. (2011). Thermal erosion of a permafrost coastline: Improving process-based models using time-lapse photography. *Arctic Antarctic and Alpine Research*, 43(3), 474–484. <https://doi.org/10.1657/1938-4246-43.3.474>
- Yu, Y., Stern, H., Fowler, C., Fetterer, F., & Maslanik, J. (2014). Interannual variability of Arctic landfast ice between 1976 and 2007. *Journal of Climate*, 27(1), 227–243. <https://doi.org/10.1175/JCLI-D-13-00178.1>